Indian Journal of Pure & Applied Physics
Vol. 53, November 2015, pp. 718-724

Improved photoresponse of porous silicon photodetectors by embedding CdSe nanoparticles

Nadir F Habubi[1], Raid A Ismail[2]*, Ahmed N Abd[1] & Walid K Hamoudi[2]

[1]Physics Department, Faculty of Education, University of Al-Mustansiriyah, Baghdad, Iraq

[2]Department of Applied Sciences, University of Technology, Baghdad, Iraq

[3]Physics Department, Faculty of Science, University of Al-Mustansiriyah, Baghdad, Iraq

*E-mail: raidismail@yahoo.com

Received 28 May 2015; revised 25 July 2015; accepted 23 September 2015

The paper presents the effect of incorporating colloidal cadmium selenide nanoparticles on the characteristics of porous silicon Al/porous Si/*p*-Si photodetectors prepared with 7 mA/cm^2 electrochemical etching for 15 min. The spherical cadmium selenide nanoparticles of size 35-60 nm, synthesized by laser ablation in methanol, had covered the pore walls of porous silicon matrix. Structural, morphological and optical properties of porous silicon and cadmium selenide nanoparticles were characterized by X-ray diffraction, photo-luminescence, Fourier transformation infrared spectroscopy, scanning electron microscopy, transmission electron microscopy, atomic force microscopy and UV-Vis spectrophotometer. Electrical and photosensitivity of porous silicon photodetectors have been investigated before and after the embedding of cadmium selenide nanoparticles. The ideality factor of porous silicon has decreased after the incorporation of cadmium selenide nanoparticles in porous silicon. Photodetector sensitivity has increased from 0.5 to 0.8 A/W at 800 nm after embedding CdSe NPs in silicon pores.

Keywords: Laser ablation, Porous silicon, Photodetector, CdSe, Nanoparticles

1 Introduction

Cadmium selenide (CdSe) has received much attention due to their photovoltaic, photo-electro-chemical (PEC) and electroluminescent properties[1-4]. CdSe is a semiconductor having a band gap E_g of 1.7 eV at 300 K and lies in the solar energy spectrum[5]. CdSe has been considered in many applications such as optoelectronic devices[6], light sensors[7], biological labels[8], chemical libraries[9], etc. The CdSe nanoparticles can provide superior and unique properties depending upon their shape and size[10-13]. Hydrothermal, sol–gel approach, surfactant-assisted approach, laser ablation in liquid etc. have been utilized for the synthesis of CdSe nanoparticles[14-16]. The fabrication and characterization of porous silicon photodetector have been studied by researchers[17-19]. The reported data showed low photosensitivity of porous silicon photodetector as compared to standard single crystal junction silicon photodetectors. The photosensitivity of *p*-type porous silicon photodetector was improved after doping the pores with colloidal CdSe/CdS/ZnS quantum dots due to large surface areas and short diffusion length of photo-generated carriers[20]. The doping of CdSe nanoparticles in porous silicon photodetector to improve its photosensitivity, has been studied in the present paper.

2 Experimental Details

Mirror-like single crystal (2-20) Ω.cm, 508 μm thick and (100) *p*-type silicon wafers were cleaned, cut into (1.5×1.5) cm^2 rectangles and then chemically treated with HF. The aluminium ohmic contacts of 1 μm thickness were deposited on the backsides of the wafer by using thermal resistive technique, and anti-acid wax layer was then applied to protect this electrode during electrochemical etching. The porous layer was obtained by electrochemical etching of the silicon samples in 1:1 mixture of HF (40%)-ethanol (99.99%) solution using 7 mA/cm^2 current density at room temperature for 15 min. After anodization, the silicon samples were washed out with deionized water for 10 min and dried under N_2 ambient. Teflon electrochemical etching cell employing Au grid was used in the current study and is shown in Fig. 1. The etched area was adjusted to be around 0.8 cm^2.

Cadmium selenide nanoparticles NP_S were produced by laser ablation of high purity CdSe 1 cm^2 pellet in 99.99% purity methanol CH_4O (provided by Poch Company) at room temperature. The CdSe

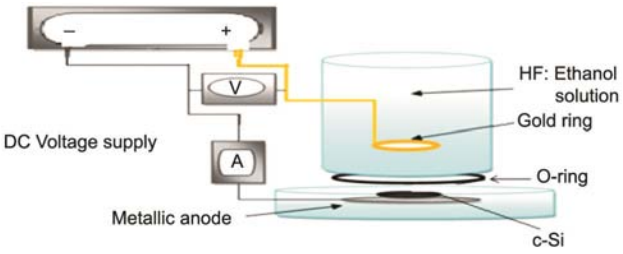

Fig. 1 — Schematic diagram of the electrochemical etching experimental set-up

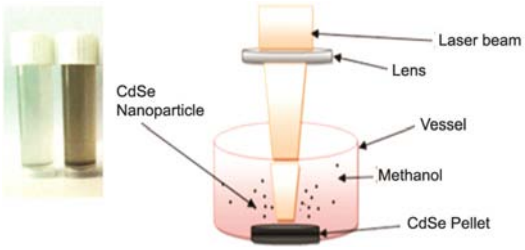

Fig. 2 — Laser ablation in liquid system. inset is fresh colloidal CdSe NPs

target was placed in the bottom of quartz vessel and a colloidal CdSe NPs solution was made to fill this vessel up to 5 ml above the target. The colloidal solution was synthesized by irradiating of CdSe pellet with 7 ns pulsed Nd: YAG laser operating at λ=1064 nm (type HUAFEI). A positive 20 cm lens was employed to focus laser beam onto target. The laser fluence of 1 J/cm^2 and ablation time of 5 min were set to carry out this experiment. The schematic diagram of laser ablation in liquid system is shown in Fig. 2.

Structural, morphological and optical properties of porous silicon and CdSe NPs were investigated by means of (CuKα) XRD-6000, Shimadzu X-ray diffractometer, Shimadzu SL 174 PL spectrophotometer, Fourier transformation infrared spectroscopy, JEOL (JSM-5600) scanning electron microscopy, Philips CM10 pw 6020 transmission electron microscopy, Angstrom AA 3000 atomic force microscopy and Cary 100 Conc plus UV-Vis spectrophotometer. The colloidal CdSe nanoparticles with concentration of around 10 mg/mL were embedded in porous silicon by drop casting technique.

The photosensitivity was measured by utilizing a monochromator and the power was calibrated using Sanwa silicon power meter. The photogenerated minority carrier lifetime of the heterojunction was measured using stroboscope and oscilloscope of

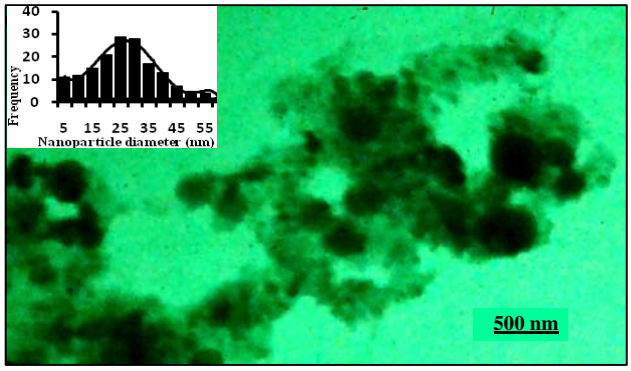

Fig.3 — TEM image of CdSe colloidal nanoparticles suspended in methanol. The inset shows the particles size distribution histogram

100 MHz band width. All the above characteristics have been investigated at room temperature.

3 Results and Discussion

3.1 Synthesis of cadmium selenide nanoparticles formation

The solution colour has changed to dark brown after laser ablation of CdSe target; indicating the formation of CdSe NPs, see inset of Fig. 2.

The micrograph of CdSe nanoparticles TEM images, shown in Fig. 3, confirms the formation of nearly spherical, 25-30 nm mono-dispersed CdSe nanoparticles. The CdSe particle size distribution histogram was determined using software supported TEM analysis as shown in the inset of Fig. 3. It is Gaussian with the full width at half maximum FWHM of 25 nm. Figure 4 shows SEM images of CdSe nanoparticles, revealing non-uniform CdSe nanoparticles morphology; consisting of many small irregular (35-60 nm) nanoparticles.

Different sizes were produced from different laser energy fluences. The higher magnification SEM image (inset of Fig. 4) displaying CdSe NPs agglomerated in clusters to form larger particles. NPs agglomeration is affected by the solution type and laser-nanoparticles interaction[21].

Figure 5 shows 3D AFM image of the synthesized CdSe NPs showing vertically aligned closely packed ball-shaped grains of CdSe NPs distributed uniformly within the scanning area 500×500 nm. Using special software, the estimated root mean square (RMS) surface roughness was around 0.11 nm.

The XRD diffraction patterns of synthesized CdSe nanoparticles films ablated in methanol is shown in Fig. 6. It reveals the main peaks at diffraction angle of 23.67°, 25.35°, 27.08°, and 35.19° correspond to

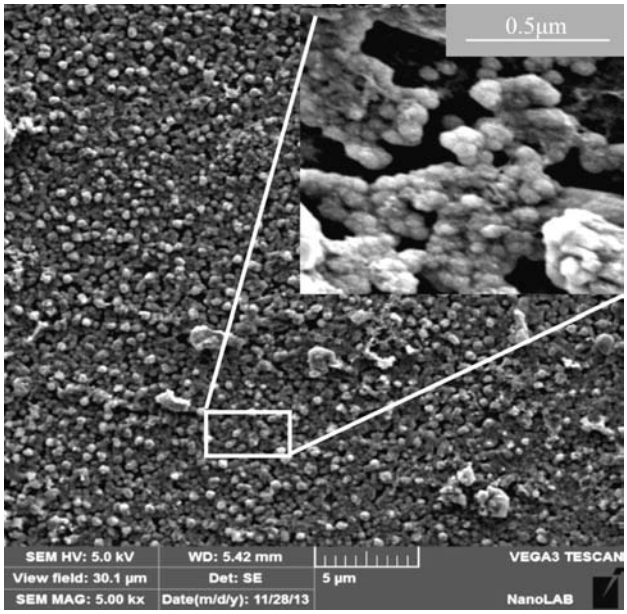

Fig. 4 — SEM image of CdSe NPs. The inset is CdSe particles agglomerated from many nanoparticles

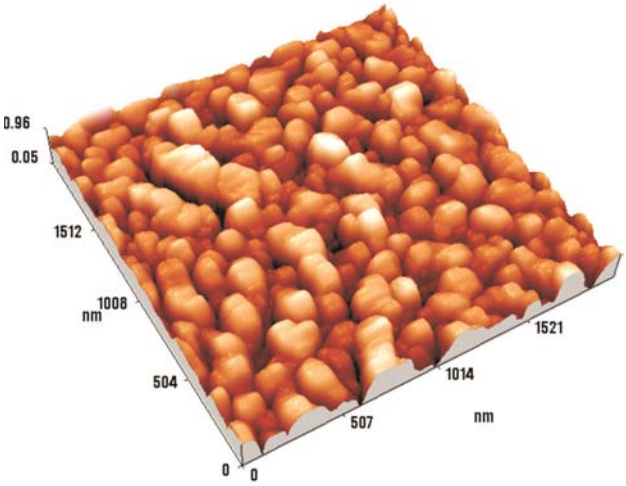

Fig. 5 — 3D AFM image of the synthesized CdSe NPs

(100), (200), (101), and (102) planes, respectively. All the diffraction peaks are indexed to the hexagonal structure with no traces of cubic face. These peaks match well the standard peaks[22] (JCPDS No. 77-2307). The average crystallite size of CdSe nanoparticles was calculated by using Scherrer formula[23] and found to be 63 nm, which is in agreement with those determined from TEM and SEM investigations.

The absorption characteristics can be a valuable tool for analyzing nanomaterials. Figure 7 shows the absorption spectrum of laser-ablated CdSe NPs in

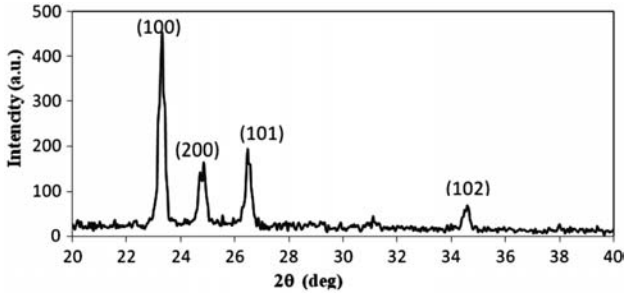

Fig. 6 — XRD pattern of CdSe nanoparticles

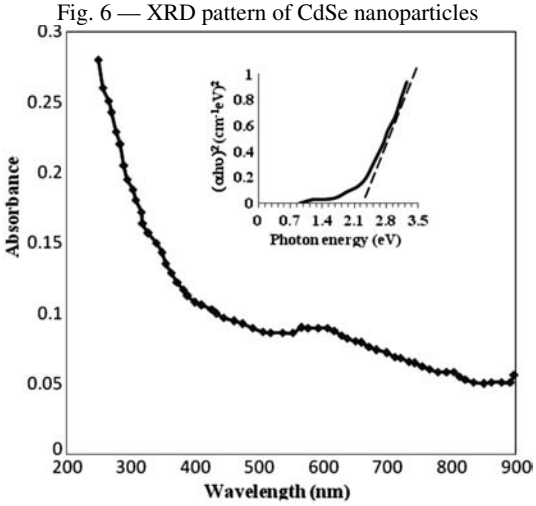

Fig. 7 — Absorption spectrum of colloidal CdSe NPs. Inset is $(\alpha h\nu)^2$ versus photon energy

suspension. The data are corrected for solution absorption in UV region. The absorption is sharply decreasing below ~ 400 nm because of the wide distribution of particle sizes[24]. The presence of a wide absorption peak around 600 nm arises from the quantum size effect; ascribed to the formation of CdSe nanoparticles.

The energy band gap of CdSe NPs was estimated by plotting $(\alpha h\upsilon)^2$ versus $(h\upsilon)$. The extrapolation of the straight line to $(\alpha h\upsilon)^2 = 0$ points gives optical energy gap as shown in inset of Fig. 8. The direct type transition is also shown with CdSe NPs band gap of 2.3 eV; which is larger than that for bulk[25] CdSe 1.7 eV. This is 0.6 eV blue shift originated from the quantum size effect indicating that the CdSe nanoparticles were successfully prepared in the present study.

3.2 Morphological and Structural Properties of Porous Silicon (PSi)

The silicon microstructure of the samples prepared with 7 mA/cm^2 current density and 15 min etching time was investigated using AFM, XRD, FT-IR, and

SEM techniques. The surface morphology of the PSi/*p*-Si layer, investigated by the AFM, showed porous structure consisting of a matrix of random distrusted nanocrystallite pillar silicon having the same direction as shown in Fig. 8. The root mean square RMS surface roughness was estimated from AFM investigations after using special software and found to be 0.7 nm. Figure 9 is an X-ray diffraction spectra showing distinct variation between fresh [Fig. 9(a)] and porous [Fig. 9(b)] silicon PSi surfaces. A strong peak at $2\theta = 69.7°$, corresponds to (400) plane is observed confirming the mono-crystalline structure of the PSi layer which belongs to the (400) reflecting plane of Si of cubic structure. The broadening in the diffracted peaks is due to the formation of nanostructured silicon layer. The upward shift may be ascribed to relaxation of strain in the porous structure[26].

The FT-IR spectrum of PSi is shown in Fig. 10. The peak at 1080 cm^{-1} indicates the presence of Si-O-Si wagging and the small peak at 624 cm^{-1} is assigned to the Si-H Waggener mode, while, the peak at 2854 cm^{-1} suggests a C-H stretching. A strong broad band seen at about 1080 cm^{-1} is due to the Si-O-Si asymmetrical stretching vibration of porous silicon. The weak absorption bands centered at about 624 cm^{-1} are attributed to the wagging modes of the SiH_x species. Absorption peaks at 2854 cm^{-1} and 2924 cm^{-1} are due to the plane C–H angle deformation. The latter can easily replace a silicon atom to allow the presence of carbon in the porous structure since carbon is located in the same column of the periodic table as silicon[27]. Upon anodization in air, new chemical bonds appear on the surface as a wide transmission band due to different Si-H and Si-O chemical bond configurations in the IR spectra.

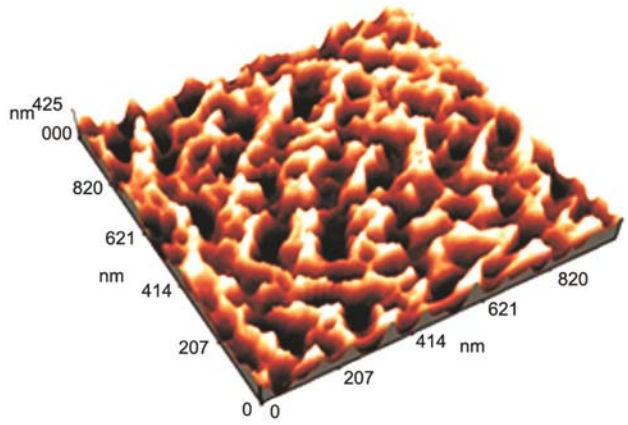

Fig. 8 — 3D AFM image of porous silicon

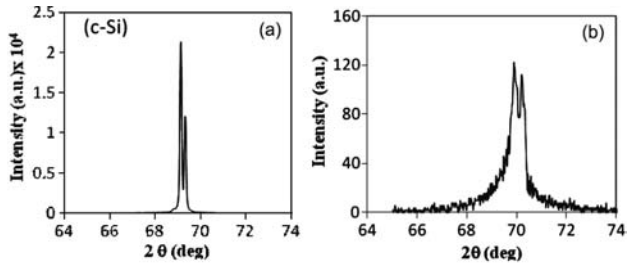

Fig. 9 — XRD spectra of (a) mono-crystalline silicon surface and (b) porous silicon surface

3.3 CdSe/PSi/Si Heterojunction Photodetector Properties

Figure 11 shows CdSe NPs deposited on a porous silicon surface specified by 250-400 nm semi-circular pores (inset of Fig. 11). Bigger CdSe particles are agglomerated as multi – armed or cubic shape on the porous surface. Particles smaller than the pore size are embedded inside the silicon matrix. The porosity was estimated and found to be around 75%.

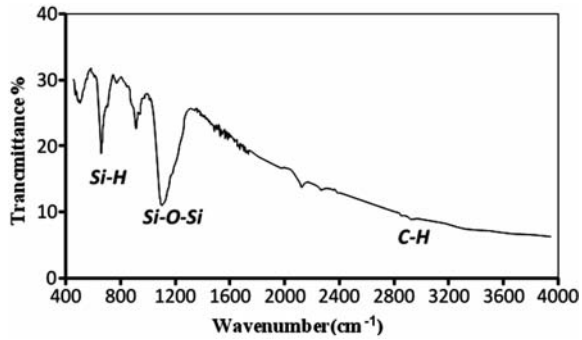

Fig. 10 — FT-IR spectrum of the porous silicon

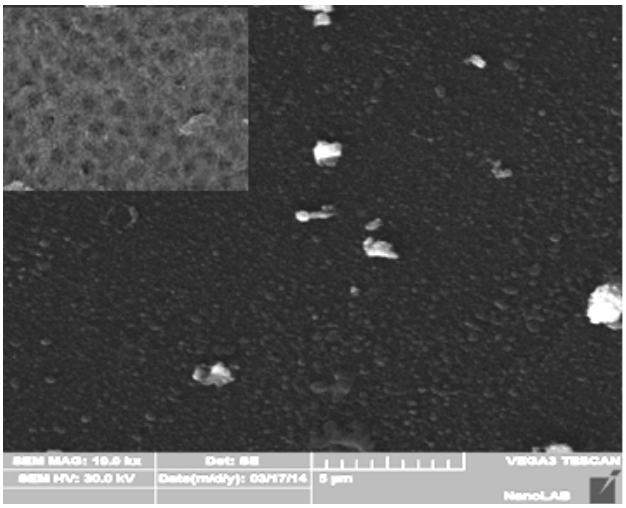

Fig. 11 — SEM images of CdSe nanoparticles within the pores of porous silicon matrix. Inset is porous silicon surface

Figure 12 shows the dark *I-V* characteristics in forward and reverse directions of Al/CdSe/PSi/p-Si/Al and Al/PSi/p-Si photodetectors. *I-V* characteristics exhibited rectification properties. The forward current of porous photodetector has increased after embedding CdSe NPs. This indicates some improvement in the charge transfer between porous and electrode after CdSe doping..

To calculate the ideality factor, a semi-logarithmic relationship of forward current versus bias voltage is plotted as shown in Fig. 13. The values of ideality factor of heterojunction are found to be 3.6 before doping and 1.4 after CdSe NPs doping. The decrease in ideality factor values indicates a significant enhancement of the porous heterojunction performance after the CdSe NPs doping. This may well be resulted from the increase of porous layer shunt conductivity after diffusing CdSe NPs in the silicon matrix.

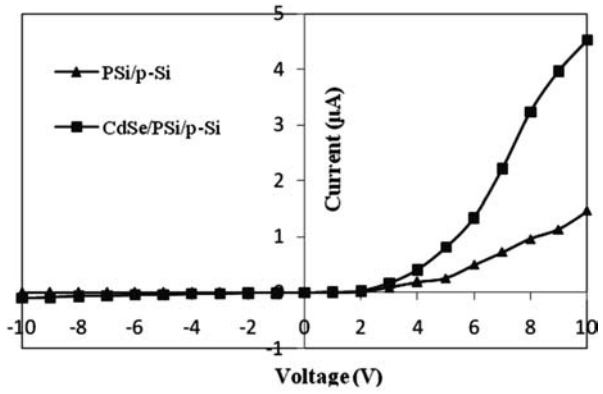

Fig. 12 — Dark *I-V* characteristics of Al/CdSe/PSi/*p*-Si/Al and Al/PSi/p-Si heterojunctions

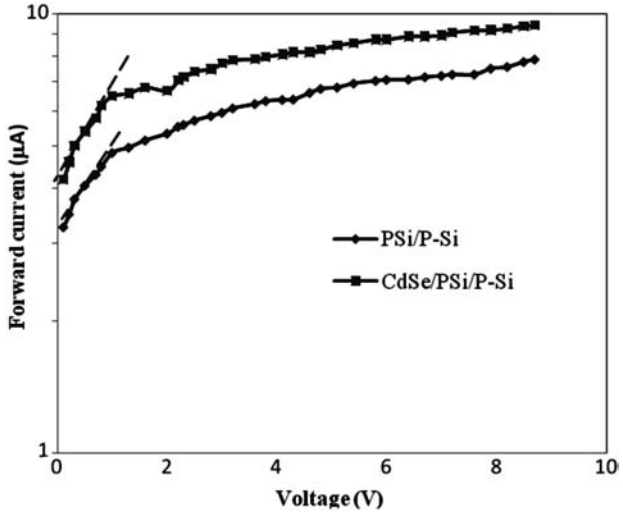

Fig. 13 — Semi-logarithmic of forward current versus bias voltage plot

Figure 14 shows *I-V* characteristics of porous silicon photodetectors before and after embedding CdSe under 10 mW/cm^2 white light illumination, indicating an increasing photocurrent after CdSe doping. This increase could be due to the increase of absorption coefficient and carriers' diffusion length and/or the photo-induced carriers transfer from CdSe NPs to porous silicon caused by band alignment between CdSe and porous silicon. These results agree well with data reported in Ref. (20). Figure 15 shows a liner relationship between inverse of square of capacitance C^{-2} reverse bias voltage for doped and un-doped heterojunction, indicating abrupt junctions. The built-in potential V_{bi} values were obtained after extrapolating the C^{-2} points to voltage axis. V_{bi} has decreased from 1.05 to 0.5V after doping. This result agrees with the results of dark *I-V*. The dark *I-V* characteristics revealed a decreased turn-on voltage after doping with CdSe NPs.

Figure 16 shows the photosensitivity of CdSe/PSi/*p*-Si and PSi/*p*-Si photodetectors at 1V bias voltage. Before doping, the photosensitivity has two peaks located at 600 nm (due to the absorption edge of porous layer) and 800 nm (related to the absorption of light in the bulk silicon substrate). Adding CdSe,

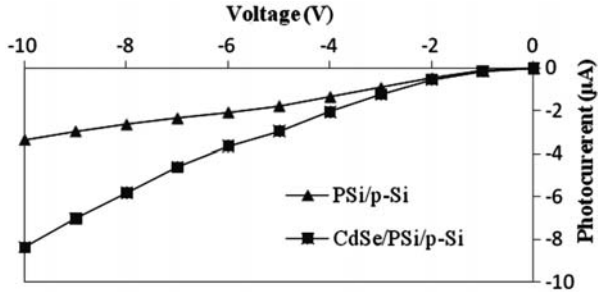

Fig. 14 — Illuminated *I-V* characteristics of CdSe/ PSi/*p*-Si and PSi/*p*-Si photodetectors

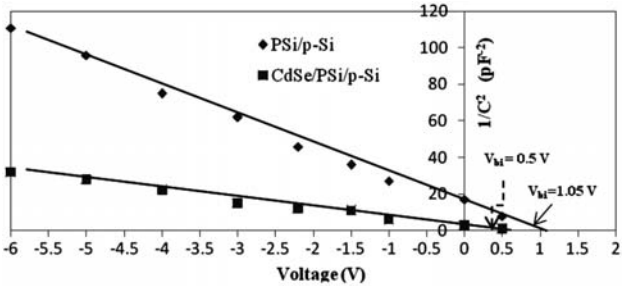

Fig. 15 — Effect of CdSe doping on the characteristics of C^{-2} versus reverse voltage

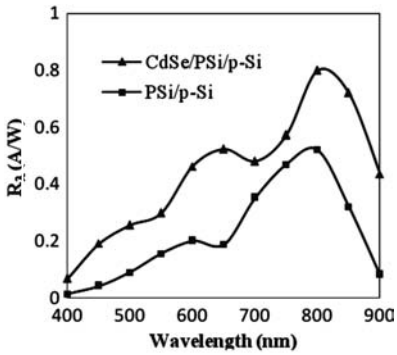

Fig. 16 — Doping effect of CdSe NPs on the photodetector photosensitivity

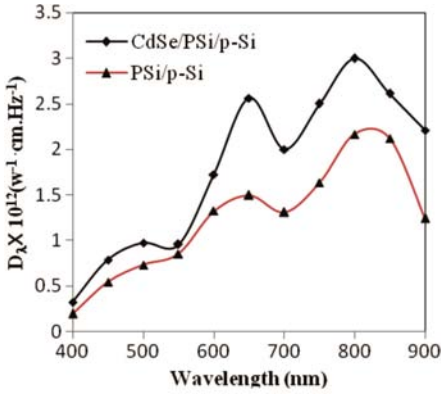

Fig. 17 — Detectivity as function of wavelength of photodetectors before and after doping

NPs has significantly enhanced the photosensitivity reaching maximum of 0.8 A/W at 800 nm. Another response peak, located at 560 nm can be ascribed to the absorption edge of CdSe nanoparticles. The obtained value of photosensitivity is higher than that for other porous and heterojunctions based silicon photodetectors[28-30]. Figure 17 shows the specific detectivity (D^*) as a function of wavelength before and after doping, with a maximum value of 2.3×10^{12} $W^{-1}.cm.Hz^{1/2}$ found at 750 nm for CdSe/PSi/p-Si photodetector. These data reported here have shown repeatability over several runs and over several samples.

Open circuit voltage decay OCVD method was used to measure the photo-generated minority carrier life time τ of the photodetectors. Figure 18 shows an optical response of 20 mW/cm^2 light pulse. The lifetime[31] was calculated by using Eq. (1):

$$\iota = \left(\frac{2kT}{q}\right)\left[\frac{1}{dV_{OC}/dt}\right] \quad \ldots(1)$$

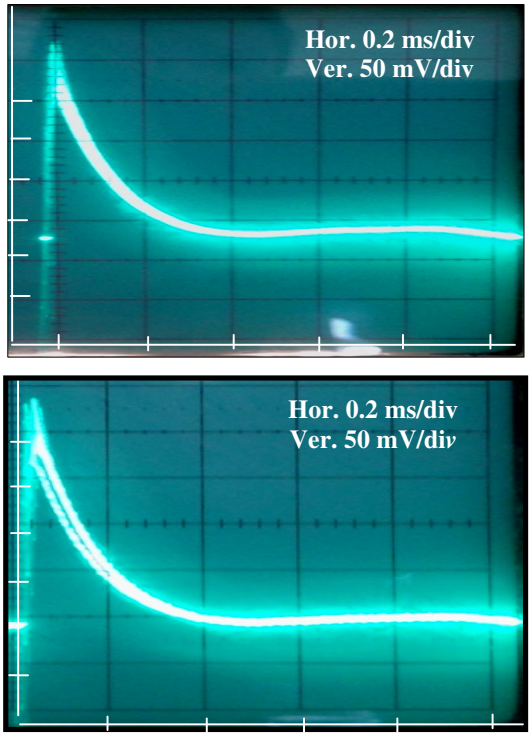

Fig. 18 — Optical response pulse for heterojunctions before doping (top) and after doping of CdSe NPs into silicon matrix (bottom)

The estimated lifetime of heterojunction photodetector increased from 124 μs to 320 μs after doping indicating improved heterojunction photovoltaic characteristics after doping because of the structural and surface states defects decrease at the PSi-*p*-Si interface.

4 Conclusions

A simple and efficient approach to improve the photo-response and photovoltaic properties of silicon matrix photodetectors prepared by anodization technique via doping with colloidal CdSe nanoparticles, synthesized by laser ablation in methanol, is presented. The enhancement in photo-response and photovoltaic properties was explained by the increasing the absorption coefficient and carrier diffusion length as well as by the carrier transfer from CdSe NPs to porous silicon. Larger direct 2.3 eV bandgap transition than that for bulk CdSe 1.7 eV was obtained, indicating a successful CdSe NP preparation. The results showed a mono-crystalline porous structure of random distrusted nanocrystallite pillar silicon having same direction. *I-V* characteristics indicated an improved charge

transfer between porous and electrode and an increased photocurrent after CdSe doping. The decrease in ideality factor from 3.6 to 1.4, enhanced photosensitivity to 0.8 A/W, high specific detectivity of 2.3×10^{12} $W^{-1}\cdot cm.Hz^{1/2}$ at 750 nm and increased heterojunction life time from 124 μs to 320 μs point out a significant enhancement of the porous heterojunction performance after the CdSe NPs doping. The high photosensitivity at visible and near-IR regions suggests using this route to fabricate silicon photodetectors to detect weak optical signals.

References

1 Murali K R, Swaminathan V & Triverdi D C, *Sol Energy Materials & Solar Cells*, 113 (2004) 81.
2 Hahn D, Mishra K K & Rajeshwar K K, *J Electrochem Soc*, 100 (1991) 138.
3 Mishra K K & Rajeshwar K K, *J Electroanal Chem*, 273 (1989) 169.
4 Murali K R, Subramanian V, Ransgarajan N, Laskshmanan A S & Rangarajan S K, *J Electroanal Chem*, 368 (1994) 95.
5 Kale R B & Lokande C D, *Semicond Sci Techol*, 1 (2005) 120.
6 Nazzal AY, Qu L, Peng X & Xiao M, *Nano Letter*, 3 (2003) 819.
7 Bruchez M, Moronne M, Gin P, Weiss S & Alivisatos A P, *Science*, 281 (1998) 2013.
8 Colvin V L, Schlamp M C & Alivisatos A P, *Nature*, 370 (1994) 354.
9 Gaponik N, Radtchenko I L, Sukhorukov G B & Rogach A L, *Adv Mater*, 12 (2002) 879.
10 Haram S K, Quinn B M & Bard A J, *J Am Chem Soc*, 123 (2001) 8860.
11 Wang Z L, Kong X Y, Ding Y, Gao P, Hughes W L, Yang R & Zhang Y, *Adv Function Mater*, 14 (2004) 943.
12 Datta S & Das B, *Appl Phys Lett*, 56 (1990) 665.
13 Peng X G, Manna L, Yang W D, Wickham J, Scher E, Kadavanich A & Alivisatos A P, *Nature* 404 (2000) 59.
14 Tang K B, Qian Y T, Zeng J H & Yang X G, *Adv Mater*, 15 (2003) 448.
15 Busbee B D, Obare S O & Murphy C J, *Adv Mater*, 15 (2003) 414.
16 Abd A, Habubi N & Raid A Ismail, *J Mater Sci Mater Electron*, 25 (2014) 3190.
17 Raid A Ismail, *J Surf Sci Nanotech*, 8 (2010) 388.
18 Lee M K, Nat Sun Yat-Sen, Wang Y H & Chu C H, *Quantum Electronics IEEE*, 33 (1997) 2199.
19 J Kim, S Joo, Kyeong W Lee, J Kim, D Shin, S Kim & S Cho, *ACS Appl Mater Interfaces*, 6 (2014) 20880.
20 Chia-Man Chou, Hsing-Tzu Cho, Vincent K S Hsiao, Ken-Tye Yong & Wing-Cheung Law, *Nanoscale Res Lett*, 7 (2012) 291.
21 Z Yan, R Bao, C Dinu,Y Huang, A Caruso & D Chrisey, *J of Optoelectronics & Adv Materials*, 12 (2010) 437.
22 JCPDS-International centre for diffraction data (1998) USA card No 77-2307.
23 Scherrer P, *Göttinger Nachrichten Gesell*, 2 (1918) 98.
24 Albert A Ruth & John A Young, *Colloids & Surfaces A*, 279 (2006) 121.
25 Chate P A, Sathe D J, Hankare P P, *J Mater Sci Mater Electron*, 22 (2011) 111.
26 Dwivedi K, Kumar V, Dubey M & Pathak H P, *Chalcogenide Lett*, 8 (2011) 521.
27 Koropecki R R & Arce R, *J Appl Phys*, 60 (1986) 1802.
28 Raid A Ismail, Yaha Khalid Z & Abdulrazaq Omar A, *Surface Rev & Lett*, 12 (2005) 299.
29 Kuen-Hsien Wu, *J of Nanomaterials*, 2014 (2014) 56527.
30 Raid A Ismail, *J of Semicon Tech & Sci*, 6 (2006) 119.
31 John E M, Thomas W E, Robert I F & Roy K, *IEEE Trans on Electron Dev*, 26 (1979) 733.